Evidence for core excitation in single-particle states of ^{19}Na

M.G. Pellegriti, N.L. Achouri, C. Angulo, J.C. Angélique, E. Berthoumieux, E. Casarejos, M. Couder, T. Davinson, C. Ghag, A.St. Murphy, et al.

Evidence for core excitation in single-particle states of ^{19}Na

M.G. Pellegriti [a,1], N.L. Achouri [b], C. Angulo [a,2], J.-C. Angélique [b,3], E. Berthoumieux [c], E. Casarejos [a,4], M. Couder [a,5], T. Davinson [d], C. Ghag [d], A.St. Murphy [d], N.A. Orr [b], I. Ray [e], I.G. Stefan [e], P. Descouvemont [f,6]

[a] *Centre de Recherches du Cyclotron and Institut de Physique Nucléaire, Université catholique de Louvain, B-1348 Louvain-la-Neuve, Belgium*

[b] *LPC Caen, ENSICAEN, Université de Caen, CNRS/IN2P3, 14050 Caen Cedex, France*

[c] *DAPNIA/SPhN, Bat. 703, CEA, Gif sur Yvette Cedex, France*

[d] *School of Physics, The University of Edinburgh, Edinburgh EH9 3JZ, UK*

[e] *GANIL, Boulevard Becquerel, F-14000 Caen, France*

[f] *Physique Nucléaire Théorique et Physique Mathématique CP229, Université Libre de Bruxelles, B-1050 Brussel, Belgium*

Abstract

We present an experimental study of ^{19}Na states in the excitation energy range between 2 and 3 MeV. The presence of ^{19}Na single-particle levels at these energies was first predicted by a microscopic cluster model and then experimentally confirmed by measuring the elastic and inelastic scattering of a 66 MeV ^{18}Ne radioactive beam on a $(CH_2)_n$ target. The H(^{18}Ne,p)^{18}Ne(g.s.) and H(^{18}Ne,p')^{18}Ne*(2^+, 1.887 MeV) cross sections have been obtained in the laboratory angular range $\theta_{lab} = 6.1° - 18.4°$ and analyzed by using the R-matrix method. Two new states in ^{19}Na have been observed at centre of mass energies $E_{\mathrm{c.m.}} = 2.78 \pm 0.01$ MeV and 3.09 ± 0.05 MeV. Both resonances exhibit large widths in the ^{18}Ne(2^+)+p channel, and low branching ratios into the elastic channel. The reduced proton widths confirm the single-particle nature of these states, with a ^{18}Ne(2^+)+p structure.

Key words: elastic scattering, inelastic scattering, single-particle states
PACS: 25.60.-t, 25.60.Bx, 27.20.+n

1 Introduction

The existence of single-particle states [1] is well established in many stable nuclei. A single-particle state can be considered as an inert core (usually in its ground state) surrounded by a valence nucleon. The main characteristic of such a state is a large reduced width, close to the Wigner limit. The concept of single particle states can be extended in two directions: to nuclei near or beyond the drip lines, and to specific states where the core nucleus is in an excited state.

The aim of the present letter is to investigate the ^{19}Na spectrum above 2 MeV by inverse elastic and inelastic scattering of a ^{18}Ne radioactive beam on a proton target. In a previous experiment [2], we considered the low-energy region and found evidence for a new $1/2^+$ level ($\ell = 0$) at $E_{\mathrm{c.m.}} = 1.06$ MeV. This state is characterized by a strong Coulomb shift, consistent with a large reduced width. Its interpretation as a ^{18}Ne(0^+)+p single-particle state was confirmed in subsequent experiments [3,4].

In this work, we have investigated simultaneously the ^{18}Ne+p elastic and inelastic scattering, to search for mirror states of ^{19}O. The mirror ^{19}O nucleus is stable against neutron decay ($\tau_{1/2} = 27\ s$) and has been studied in various experiments and theoretical models (see for example Refs. [5,6]). Calculations based on a microscopic cluster model suggest that states with large ^{18}O(2^+)+n or ^{18}Ne(2^+)+p components are expected above 2 MeV excitation energy. Such states cannot be easily observed in elastic scattering, but are expected to show up in the H(^{18}Ne,p')^{18}Ne* inelastic cross section, where ^{18}Ne is in its first excited state (1.887 MeV, 2^+). The existence of core excitations in single-particle states is predicted by theory in several nuclei, and it is in that context that the present work was undertaken.

2 Microscopic calculation

Before running the experiment we have performed a preliminary calculation using a microscopic cluster model [7], based on the Generator Coordinate

---

[1] Present address: Dipartimento di Fisica e Astronomia, Universit di Catania and Laboratori Nazionali del Sud - INFN, Catania, Italy.
[2] Present address: Tractebel Engineering (SUEZ), Avenue Ariane 7, 1200 Brussels, Belgium.
[3] Present address: LPSC, Grenoble, France.
[4] Present address: Universidade de Santiago de Compostela, Spain.
[5] Present address: University of Notre Dame, South Bend, U.S.A.
[6] Directeur de Recherches FNRS.

Method (GCM) [8]. In this model, all nucleons are taken into account, and the Hamiltonian is given by

$$H = \sum_{i=1}^{19} T_i + \sum_{i>j=1}^{19} V_{ij}, \tag{1}$$

where T_i is the kinetic energy of nucleon i, and V_{ij} is a nucleon-nucleon interaction, taken here as the Volkov V2 force [9].

The GCM wave functions of ^{19}Na are factorized into ^{18}Ne and p internal wave functions as

$$\psi = \sum_k \mathcal{A}\phi_{18}^k \phi_p g_k(\rho), \tag{2}$$

where k labels the channels, $\mathcal{A}$ is the antisymmetrization operator, ϕ_{18}^k are shell-model wave functions of ^{18}O/^{18}Ne and g_k are radial functions depending on the relative coordinate ρ. All *sd*-shell states are included in the ^{18}O/^{18}Ne wave functions, in particular the 0^+ ground state, and the 2^+ first excited state (see Ref. [10] for details). The angular momentum projection is performed using standard methods [7]. This model has been used to investigate many nuclei and reactions (see for example Ref. [11]), and is well adapted to exotic nuclei with low level densities.

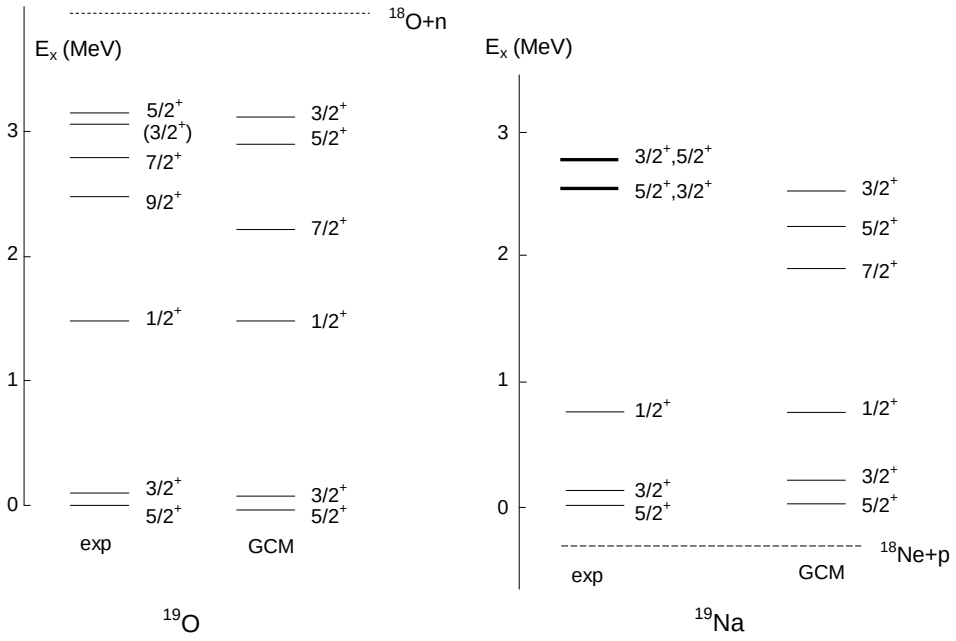

Fig. 1. GCM and experimental ^{19}O and ^{19}Na spectra. The ^{19}Na states in bold were observed in the present experiment. The particle thresholds are shown as dashed lines.

In Fig. 1, we present the ^{19}O and ^{19}Na spectra obtained from the GCM calculations. In both systems, the admixture parameter M of the Volkov force has been determined from the experimental $1/2^+$ energy. All other energies were obtained without any fitting. The low-lying part of both spectra is remarkably well reproduced by the GCM. The proton widths in the ^{18}Ne(0^+)+p and ^{18}Ne(2^+)+p channels (referred to by the indices "0" and "2", respectively) are given in Table 1, as are the angular momenta ℓ_0 and ℓ_2. Since the 2^+ excitation energy is slightly underestimated by the GCM (1.54 MeV whereas experiment gives 1.88 MeV), we have corrected the Γ_2 values to account for the experimental threshold.

For the proton width of the $1/2^+$ state, the theoretical value is slightly larger than experiment (101 ± 3 keV). The large θ_0^2 obtained from the GCM confirms the single-particle structure [2]. A $7/2^+$ state is known in ^{19}O, and is predicted by the calculation, but its width in ^{19}Na is too small to make it observable.

The calculations also predict $5/2^+$ and $3/2^+$ states ($\ell = 2$ in the ^{18}Ne(0^+)+p channel) with a dominant ^{18}Ne(2^+)+p structure. As indicated by the large θ_2^2, the GCM suggests that these states can be considered as ^{18}Ne(2^+)+p single-particle states (s wave), and should show up above 2 MeV. The dominant single-particle structure makes the GCM Coulomb shifts for these new states quite important. According to their widths, they should be observable in experiments using thick targets. Fig. 1 shows that the theoretical energies of the mirror low-lying states in ^{19}O are in good agreement with experiment, although slightly underestimated. A shell-model calculation [6] with the USD interaction predicts an ^{19}O level scheme very similar to the present one. In particular, $5/2^+$ and $3/2^+$ states are suggested at $E_x = 3.2$ MeV and 3.8 MeV, respectively.

Table 1
GCM energies and widths of ^{19}Na resonances. Total widths are given in keV, and dimensionless reduced widths (at $a = 5$ fm) in %. Angular momenta in the elastic and inelastic channels are denoted by ℓ_0 and ℓ_2, respectively. The notation x^n stands for $x \times 10^n$.

J^π	$E_{\text{c.m.}}$(MeV)	ℓ_0	ℓ_2	Γ_0	Γ_2	θ_0^2	θ_2^2
$1/2^+$	1.06	0	2	130	–	30	2.6
$7/2^+$	2.18	4	2	1.5^{-5}	8.9^{-5}	1.0^{-3}	5.4
$5/2^+$	2.52	2	0	1.5	19	0.3	50
$3/2^+$	2.81	2	0	2.0	79	0.3	31

3 Experimental method

Elastic and inelastic scattering in inverse kinematics [12] of ^{18}Ne was employed to investigate ^{19}Na. The radioactive ^{18}Ne beam was delivered using the CRC-RIB facility at Louvain-la-Neuve, Belgium. The ^{18}Ne atoms were produced via the ^{19}F(p,2n)^{18}Ne reaction by bombarding a LiF target with an intense 30 MeV proton beam from the CYCLONE30 cyclotron. After being ionized to the 4^+ state in an ECR source, the ^{18}Ne beam was post-accelerated to 66 MeV by the CYCLONE110 cyclotron [13] and directed on to a 2 mg/cm^2 $(CH_2)_n$ foil. The ^{18}Ne beam was stopped 1.5 m downstream from the target in a Faraday cup equipped with a current amplifier suitable to work with low-beam currents and with an electron-suppression system. The average beam intensity on target was typically of the order of 10^6 pps. The chosen combination of beam energy and target thickness allowed us to explore the centre of mass (c.m.) energy range $E_{\mathrm{c.m.}} = 2.6-3.4$ MeV with respect to the ^{18}Ne+p threshold for both the elastic and inelastic channels. In addition, the choice of the target thickness optimized the separation between the elastic and the inelastic events.

The recoil protons were detected using a "compact disc" silicon strip $\Delta E - E$ detector array CD-PAD [14]. It allows a very clean separation between protons, α, and β particles. No signals corresponding to heavier ions were observed in the telescope. The beam energy was deduced from the most energetic protons. It agrees within $\pm$100 keV (better than 0.4%) with the nominal beam energy. The beam energy spread was less than 100 keV full width at half maximum (FWHM). The CD-PAD array was placed 11.1 cm downstream from the target and the 16 annular strips covered a laboratory angular range of $\theta_{\mathrm{lab}} = 4.7^\circ - 20.2^\circ$. The energy calibration of the detector array was performed by means of a three-line α-source (^{239}Pu, ^{241}Am, ^{244}Cm) and a precision pulser. The laboratory proton energy resolution was 55 keV for the ΔE detectors and 90 keV for the PAD detectors. The combined energy resolution was 105 keV. The proton events were selected using a gate on the $\Delta E - E$ matrix (as in Ref. [15]).

A typical proton energy spectrum is displayed in Fig. 2 for a strip located at $\theta_{\mathrm{lab}} = 17.0^\circ$. The arrows indicate the new states in ^{19}Na as observed in the inelastic channel. In the elastic channel, the proton widths are expected to be small and thus a more detailed analysis is needed to obtain the properties of the states (Section 4).

Proton events were observed at laboratory energies higher than the maximum energy of the elastic events, probably arising from reactions on the C present in the target. In order to identify, and to subtract away these background events, a measurement was made using a pure ^{12}C target (200 μg/cm^2 thick) under the same experimental conditions as the measurements with the $(CH_2)_n$ target. A

polynomial fit of the ^{18}Ne + ^{12}C yield was performed at each measured angle both for the elastic and inelastic spectra to have a smooth parameterization of the energy dependence. The background fits were normalized to the $(CH_2)_n$ yield at higher energies (above $E_{\rm lab}$ = 12 MeV in Fig. 2) where no elastic events are present.

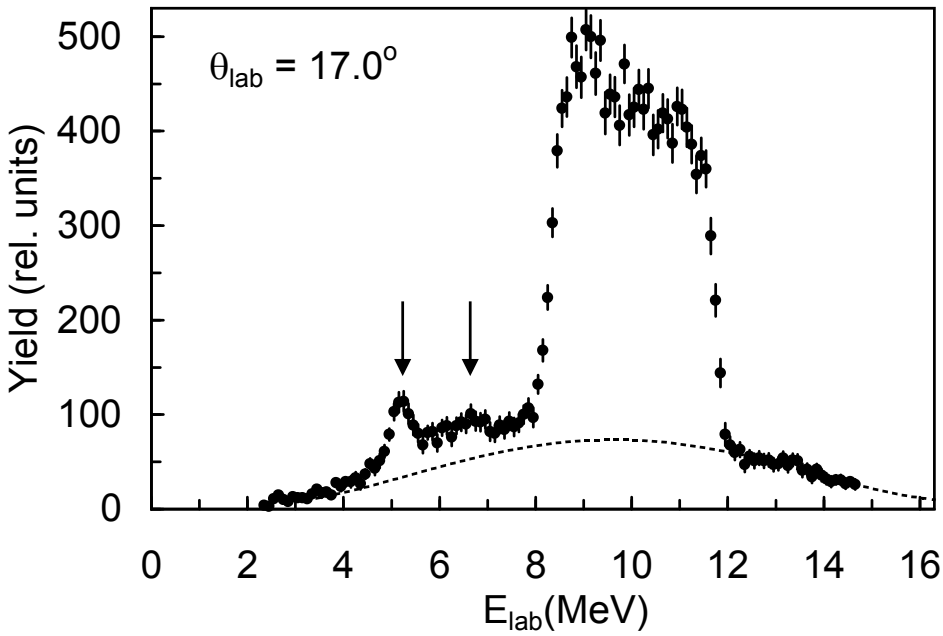

Fig. 2. Yield (in rel. units) of a 66 MeV ^{18}Ne beam on a 2 mg/cm^2 $(CH_2)_n$ target at $\theta_{\rm lab}$ = 17.0°. The two new observed ^{19}Na states are indicated by arrows. The dotted curve is a fit of the ^{18}Ne + ^{12}C background yield (see text).

Two important effects have to be taken into account in the data analysis. First, the opening angle of the detector strips introduces an uncertainty in the proton energy [16]. Typical values ranged between 25 and 100 keV (for the laboratory proton energies and angles covered). The second effect is the straggling of the beam particles and of the recoil protons in the target [17]. It produces an additional uncertainty in the laboratory energies of the recoil protons, of the order of 25 keV. The total energy broadening was obtained by combining in quadrature all contributions, and was taken into account in the theoretical analysis. The effective target thickness was obtained as a function of the beam energy by using the energy loss of ^{18}Ne in $(CH_2)_n$ [17].

The c.m. energy was calculated for both elastic and inelastic events using standard kinematic expressions [18]. In this procedure, the energy loss of the recoil protons (up to 100 keV at the lowest $E_{\rm lab}$ values) were added to the detected proton energy. The absolute elastic and inelastic cross sections were obtained for 7 effective c.m. angles (the recoil spectra of the 3 innermost strips were added three by three, the others were added two by two) in the range $\theta_{\rm lab} = 6.1° - 18.4°$ and for c.m. energies $E_{\rm c.m.} = 2.6 - 3.4$ MeV by correcting the number of counts for the solid angle of the detectors and the effective target

thickness, and by normalizing (within ±20%) to a theoretical extrapolation of previous elastic-scattering data [2,4].

In Fig. 3, the elastic and inelastic cross sections as a function of $E_{\rm c.m.}$ are shown for three typical laboratory angles: $\theta_{\rm lab} = 6.1°$, 10.7° and 16.5° ($\Delta\theta = \pm 1.5°$, $\Delta\theta = \pm 1°$ and $\Delta\theta = \pm 0.9°$, respectively). The error bars include the statistical errors, the uncertainty in the solid angles (±6%), in the effective target thickness (±5%), and from the background subtraction (±20%).

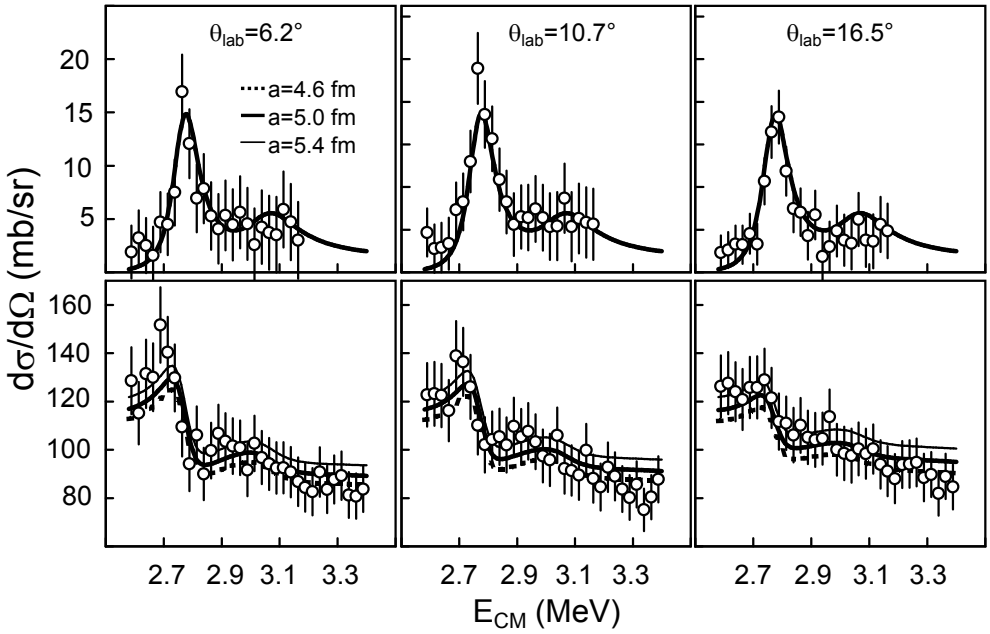

Fig. 3. Center-of-mass experimental cross section for inelastic (upper panels) and elastic (lower panels) scattering as a function of $E_{\rm c.m.}$ at three different laboratory angles. The curves are the results of the simultaneous R-matrix fits for three different values of the channel radius a. Note that at the scale of the figure, the inelastic fits are insensitive to a.

4 R-matrix analysis

The cross sections obtained here have been analyzed using the R-matrix formalism. Elastic scattering has been considered in various experiments (see for example Ref. [2]), but inelastic scattering requires some further developments. For a partial wave involving a single resonance, the 2×2 R-matrix is given by

$$R_{ij}(E) = \frac{\gamma_i \gamma_j}{E_i - E}, \tag{3}$$

where (i, j) refer to the channels, γ_i^2 are the reduced widths in the elastic ($i = 1$) and inelastic ($i = 2$) channels, and E_i is the pole energy. The transformation

between R-matrix parameters (γ_i, E_i) and "observed" parameters is done using well known techniques [19–21].

Owing to the 2^+ spin-parity of ^{18}Ne in the inelastic channel, several channel spins $(3/2^+, 5/2^+)$ and angular momenta are possible. We assume that one of them is dominant and neglect the other components. With the R-matrix (3), the collision matrix $\boldsymbol{U}$ is easily determined from Coulomb functions [19]. The element U_{11} is involved in elastic scattering, while U_{12} determines the inelastic cross sections. The elastic cross section at a c.m. angle θ is given by

$$\frac{d\sigma_{el}}{d\Omega}(E,\theta) = \frac{1}{2}\sum_{\nu,\nu'} \mid f^N_{\nu,\nu'}(E,\theta) + f^C(E,\theta)\delta_{\nu\nu'} \mid^2, \tag{4}$$

where $\nu, \nu' = \pm 1/2$ correspond to the spin orientation of the proton, and where $f^N_{\nu,\nu'}(\theta)$ and $f^C(\theta)$ are the nuclear and Coulomb amplitudes, respectively. They are given in Ref. [19] (Sec. VIII). For the inelastic cross section, we have

$$\frac{d\sigma_{in}}{d\Omega}(E,\theta) = \frac{1}{2k^2}\sum_j B_j(E) P_j(\cos\theta), \tag{5}$$

where k is the wave number, and $B_j(E)$ are the anisotropy coefficients. They are related to the collision matrix as explained in Ref. [19] (Sec. VIII).

As shown in Fig. 3 we performed a simultaneous fit of the elastic and inelastic cross sections at three different angles ($\theta_{lab} = 6.1°, 10.7°$ and $16.5°$). In other words, the 6 excitation functions of Fig. 3 were analyzed with common R-matrix parameters. Two resonances were introduced in the fit according to the experimental evidence in the inelastic events (see above). The obtained energies and widths are given in Table 2; in the R-matrix formalism, they correspond to "observed" values. The channel radius is $a = 5$ fm. The errors in the resonance parameters include the uncertainties in the experimental energy resolution and in the theoretical analysis.

Both resonances are rather broad, but the branching ratios for the decay to the elastic channel are quite small, which confirms the prediction of the GCM. In the Breit-Wigner formalism, equivalent to the R-matrix theory for a single resonance, the amplitude of the cross section at the resonance energy is proportional to $(2J+1)\Gamma_0\Gamma_2/\Gamma^2_{tot}$. As Γ_0 is much smaller than Γ_2, the physical parameter is $(2J+1)\Gamma_0/\Gamma_{tot}$. Best fits ($\chi^2/N \sim 0.4$, where $N = 171$ is the number of experimental data) are obtained with the two levels having spin assignments $(3/2^+, 5/2^+)$ or $(5/2^+, 3/2^+)$. Our experiment cannot distinguish between the two possibilities (see Fig. 4), but rules out identical spin assignments ($\chi^2/N \sim 0.8 - 0.9$).

Dimensionless reduced widths θ_0^2 and θ_2^2 can be extracted from the total widths and branching ratios. The values given in Table 2 are averages for $J = 3/2$ and $J = 5/2$. Qualitatively the experimental reduced widths are in excellent agreement with the GCM calculation. In the elastic channel, θ_0^2 is of the order of 1%, which means that this configuration is negligible. Conversely, the very large θ_2^2 values predicted by the GCM are supported by the present data, and are consistent with a single-particle structure in the ^{18}Ne(2^+)+p channel (s wave).

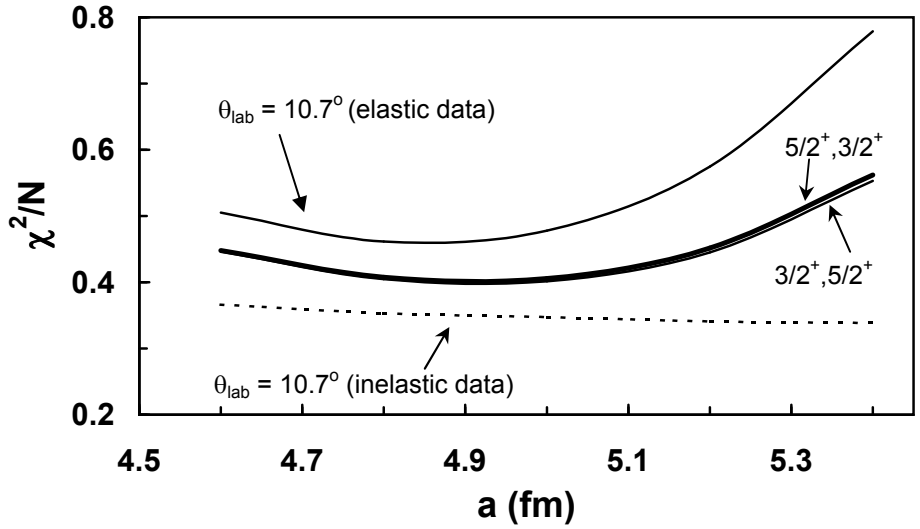

Fig. 4. Variation of χ^2 as a function of the channel radius a ($N = 171$). The two solid curves represent the global χ^2 deduced from the simultaneous fit of the inelastic and elastic data at $\theta_{\rm lab} = 6.1°$, $10.7°$ and $16.5°$. The two possible spin assignments $(3/2^+, 5/2^+)$ and $(5/2^+, 3/2^+)$ cannot be distinguished. The thin solid curve and the dotted curve are the partial χ^2 for the elastic and inelastic data ($\theta_{\rm lab} = 10.7°$), respectively.

The χ^2 dependence on the channel radius has been investigated for the global fit as well as for some individual elastic and inelastic cross sections (Fig. 4). The minimum of the global χ^2 corresponds to a channel radius near $a = 5$ fm. Both resonances are clearly characterized by $\ell = 0$ in the inelastic channel, but the total spin J cannot be determined. As shown in Fig. 4, the inelastic cross sections are virtually insensitive to the channel radius a. The main constraint is provided by the elastic scattering cross sections. This arises from interference effects between the Coulomb and nuclear contributions. In Fig. 3 we present the optimal fit for three different values of the channel radius.

The present elastic cross section is compared in Fig. 5 with data available in the literature [2,4]. Combining the three experiments provides a cross section over a wide energy range (0.7 MeV to 3.5 MeV). Slight differences in the scattering angle are not significant in view of the error bars. Owing to their dominant ^{18}Ne(2^+)+p structure, the new resonances observed here are hardly visible in the elastic data. An inelastic measurement is, therefore, necessary

Table 2
Energies and widths of ^{19}Na resonances obtained in the global R-matrix fit with $a = 5$ fm.

$E_{\mathrm{c.m.}}$ (MeV)	$2J^\pi$	Γ_{tot} (keV)	$(2J+1)\frac{\Gamma_0}{\Gamma_{\mathrm{tot}}}$	θ_0^2 (%)	θ_2^2 (%)
2.78 ± 0.03	$(5,3)^+$	105 ± 10	0.43 ± 0.05	1.1 ± 0.3	44 ± 4
3.09 ± 0.06	$(3,5)^+$	250 ± 50	0.12 ± 0.04	0.6 ± 0.2	36 ± 7

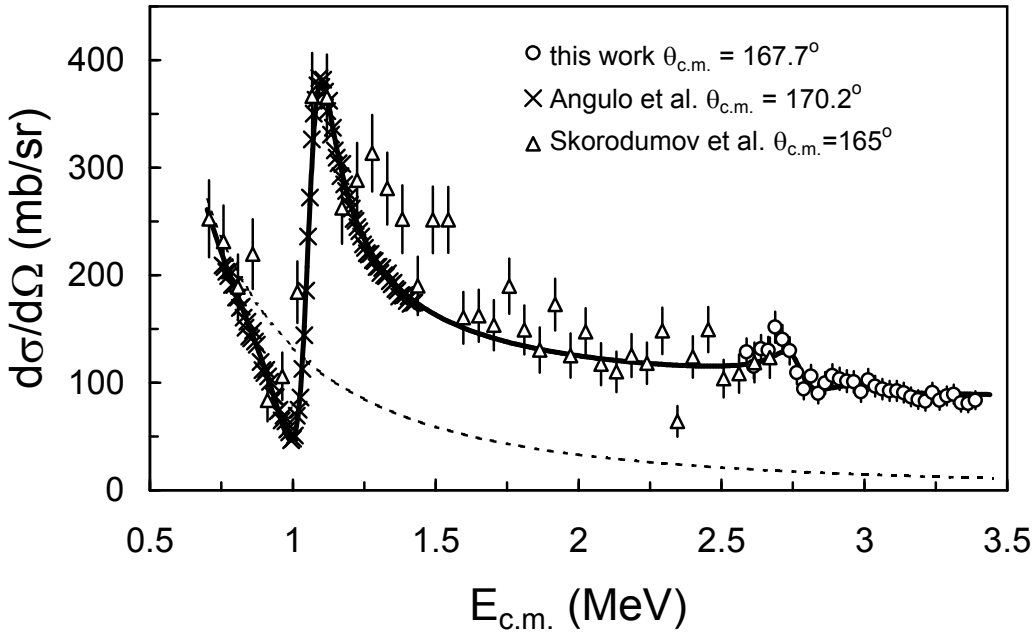

Fig. 5. Elastic cross sections from the present experiment (circles) and previous measurements [Ref. [2] (crosses) and Ref. [4] (triangles)]. The solid curve is the R-matrix calculation derived from the present analysis; the dotted curve is the Coulomb contribution to the elastic cross section (both are calculated at $\theta_{\mathrm{c.m.}} = 167.7°$).

to identify and characterize them.

5 Conclusions

The nucleus ^{19}Na has been studied in the $E_{\mathrm{c.m.}}$ range from 2.6 to 3.4 MeV by measuring ^{18}Ne+p elastic and inelastic scattering cross sections. We have observed two new states with a dominant $^{18}\mathrm{Ne}(2^+)$+p structure at $E_{\mathrm{c.m.}} = 2.78$ MeV and 3.09 MeV. In the ^{19}O mirror nucleus, several states are known in this energy region, but the spin assignments are uncertain [22]; single-particle $^{18}\mathrm{O}(2^+)$+n states are expected near $E_x \sim 3 - 3.5$ MeV.

A simultaneous R-matrix analysis of both the elastic and inelastic data allowed the total widths and branching ratios to be derived. The deduced spin-parities of the two states are $J = 3/2^+$ or $J = 5/2^+$, with identical assignments for

both excluded. The energies of these states and the large proton widths in the ^{18}Ne(2^+)+p channel are in agreement with the GCM calculation and confirm their exotic single-particle structure.

Acknowledgments

We thank the CRC staff for the production of the ^{18}Ne beam and the technical support during the experiment. This work is supported by the European Community-Access to Research Infrastructure action contract number HPRI-CT-1999-00110, and by the IAP program P6/23 initiated by the Belgian-state Federal Services for Scientific, Technical and Cultural Affairs. M.G.P. acknowledges the support of the National Fund for Scientific Research (FNRS), Belgium.

References

[1] P.G. Hansen and B.M. Sherrill, Nucl. Phys. A 693 (2001) 133.

[2] C. Angulo et al., Phys. Rev. C 67 (2003) 014308.

[3] F. de Oliveira Santos et al., Eur. Phys. J. A 24 (2005) 237.

[4] B.B. Skorodumov et al., Phys. Atom. Nucl. 69 (2006) 1979.

[5] C. S. Sumithrarachchi et al., Phys. Rev. C 74 (2006) 024322.

[6] E.K. Warburton, Phys. Rev. C 38 (1988) 935.

[7] P. Descouvemont, Nucl. Phys. A 596 (1996) 285.

[8] K. Wildermuth and Y.C. Tang, "A Unified Theory of the Nucleus", ed. by K. Wildermuth and P. Kramer, Vieweg, Braunschweig (1977).

[9] A.B. Volkov, Nucl. Phys. 74 (1965) 33.

[10] M. Dufour and P. Descouvemont, Nucl. Phys. A 726 (2003) 53.

[11] M. Dufour and P. Descouvemont, Nucl. Phys. A 785 (2007) 381.

[12] C. Angulo, Nucl. Phys. A 746 (2004) 222c, and references therein.

[13] M. Gaelens et al., Proc. of the 15th Intern. Conf. on Application of Accelerators in Research and Industry, Denton, 1998, ISBN-1-56396-825-8, p. 305.

[14] A.N. Ostrowski et al., Nucl. Instr. and Meth. Phys. Res. A 480 (2002) 448.

[15] E. Casarejos et al., Phys. Rev. C 73 (2006) 014319.

[16] R. Coszach et al., Phys. Lett. B353 (1995) 184.

[17] J.F. Ziegler, M.D. Ziegler, and J.P. Biersack, SRIM program, version SRIM-2006.02.

[18] G.R. Satchler, Introduction to Nuclear Reactions, Oxford University Press, 1990.

[19] A.M. Lane and R.G. Thomas, Rev. Mod. Phys. 30 (1958) 257.

[20] C. Angulo and P. Descouvemont, Phys. Rev. C 61 (2000) 064611.

[21] C.R. Brune, Phys. Rev. C 66 (2002) 044611.

[22] D.R. Tilley et al., Nucl. Phys. A 595 (1995) 1.